Design of a Cost-Reduced Flexible Plant for Supercritical Fluid-Assisted Applications

Cassanelli, Mattia; Prosapio, Valentina; Norton, Ian; Mills, Thomas

DOI:
10.1002/ceat.201700487

Document Version
Publisher's PDF, also known as Version of record

Citation for published version (Harvard):
Cassanelli, M, Prosapio, V, Norton, I & Mills, T 2018, 'Design of a Cost-Reduced Flexible Plant for Supercritical Fluid-Assisted Applications', *Chemical Engineering and Technology*, vol. 41, no. 7, pp. 1368-1377. https://doi.org/10.1002/ceat.201700487

Mattia Cassanelli
Valentina Prosapio*
Ian Norton
Thomas Mills

Design of a Cost-Reduced Flexible Plant for Supercritical Fluid-Assisted Applications

A novel batch plant for supercritical CO_2 applications is proposed which is not equipped with expensive components, such as high-pressure pumps, making it particularly suitable for bench-scale use. For the first time, the use of a hanging scale is suggested to weigh the amount of CO_2 required for the experiment and the use of the thermodynamics to reach the working conditions. The rig is able to cover different applications, e.g., aerogel drying, impregnation, and extraction, showing high flexibility. An approximate cost analysis has been performed considering as a reference a 150-mL vessel. It has been calculated that both the setup and running costs are considerably lower than the common batch and semicontinuous rigs.

Keywords: Batch plants, Cost reduction, Process flexibility, Supercritical CO_2

Received: August 25, 2017; *revised:* January 29, 2018; *accepted:* April 24, 2018

DOI: 10.1002/ceat.201700487

1 Introduction

Supercritical fluid-assisted techniques have gained interest due to the unique properties of supercritical fluids (SCFs). SCFs show, at the same time, liquid-like properties and gas-like properties which can be tuned according to the employed pressure and the temperature [1, 2]. Carbon dioxide (CO_2) is the most used fluid since it has a relatively accessible critical point, i.e., 304.25 K and 7.38 MPa, which makes it useful for the processing of thermosensitive compounds; moreover, it is nonflammable, nontoxic, noncorrosive, inexpensive, and can be easily recycled [3]. Supercritical CO_2 ($scCO_2$)-assisted processes have been successfully applied to several fields, e.g., aerogel drying, impregnation, and extraction.

Traditional gel drying techniques, i.e., freeze-drying and air-drying, are characterized by high energy consumption, long processing times, and/or can cause the collapse of the gel structure with consequent low porosity [4]. In this field, an innovative method consists in the hydrogel-alcogel transition, followed by solvent removal using $scCO_2$ [5]. This process is faster, allows a better retaining of the gel structure and a good control over the porosity and pore size distribution [4].

Conventional techniques for the impregnation of active compounds in a porous substrate involve organic solvent evaporation; however, high residual solvent and decomposition of thermolabile molecules may occur [6]. These problems are avoided in supercritical impregnation since organic solvents are not used, mild temperatures are applied, and at the end of the process, CO_2 is completely removed from the product by depressurization.

Traditional solid-liquid extraction requires the use of expensive and hazardous organic solvents, harmful both for living beings and the environment [7]. Supercritical CO_2 extraction overcomes this obstacle providing high-quality extracts while reducing the toxicity associated with the solvents and shortening the processing time [8].

However, supercritical fluid-assisted techniques show also some limitations, such as the need of specialized and expensive equipment and high energy costs mainly related to the fluid compression [9–11]. Therefore, their application has been restricted in the last years mainly to high-added-value products [12]. In order to extend the utilization of these technologies to other industrial fields and reduce their environmental impact, strategies aimed to overcome the above reported limitations should be suggested. In literature, many studies about the use of $scCO_2$ have been proposed for different applications [13–20], but papers regarding the design of a high-pressure plant, able to adapt to different processes, with reduced setup and running costs have not been published so far.

In this work, a novel flexible batch plant for supercritical fluid-assisted processes is proposed. The aforementioned restrictions are minimized by the absence of pumps, which are expensive for high-pressure applications and require high energy consumption. The employed vessel is not equipped with transparent windows that are used by some authors to visually observe the transition from liquid to supercritical conditions in the absence of pumps [21, 22] or to study the vapor-liquid equilibria (VLE) of the systems solvent-antisolvent and solvent-antisolvent-solute [23, 24]. To work at high pressure val-

Mattia Cassanelli, Dr. Valentina Prosapio, Prof. Ian Norton, Dr. Thomas Mills
v.prosapio@bham.ac.uk
University of Birmingham, School of Chemical Engineering, Edgbaston, Birmingham B15 2TT, UK.

ues, these windows are usually made of quartz which is a high-priced material [25].

In the present work, the supercritical conditions are attained by taking advantage of the thermodynamics of the system formed by CO_2, solute, and solvent (e.g., ethanol if present): the process is designed to achieve a specific pressure at the working temperature by calculating and weighing the precise amount of CO_2. The rig can be adapted for different applications; in particular, in the present study it has been tested for gel drying, impregnation of a porous substrate with α-tocopherol, and extraction of caffeine from green coffee beans and tea leaves. The operating principle of the designed rig will be described more in details and its applicability will be assessed. For each application, the thermodynamics of the involved system will be studied and some preliminary experiments will be performed. Finally, a setup and running cost analysis will be discussed to verify the convenience of the proposed plant compared to the classic batch and the semicontinuous ones.

2 Materials and Methods

2.1 Materials

The proposed rig was built with piping, valves, and joints purchased from Swagelok© (Manchester, UK). A pure CO_2 cylinder in a dipped-tube configuration was used to withdraw liquid CO_2 (BOC, Guildford, UK) for all the experiments in this work. For the gel drying experiments, gels were made by dissolving 2 wt % low acyl gellan gum (Kelcogel F, CPKelco, UK) in distilled water and stirring at 358 K for 2 h. The solution was then placed into cylindrical moulds and, after gelation on cooling at 20 °C, samples were 1 cm high with a 1.3 cm diameter. Absolute ethanol (EtOH, purity 99.9 %) supplied by AnalaR NORMAPUR (VWR, UK) served as a pretreatment agent. For the impregnation process, a freeze-dried gel, made of a 1:1 mixture of low-acyl (LA) and high-acyl (HA) gellan gum at 2 wt %, was used as a porous substrate. The dimensions of the dried gel were the same as mentioned for the gel drying process. Vitamin E (α-tocopherol, purity > 95.5 %), provided by Sigma-Aldrich (UK), was loaded into the dried gel during the $scCO_2$ adsorption. The caffeine extraction process was performed on both coffee beans (green robusta coffee beans) and black tea leaves. Pure caffeine (purity 99 %), supplied by Sigma-Aldrich (UK) was used as a reference standard.

2.2 Rig Description and Procedure

The outline of the proposed rig is shown in Fig. 1. Section 1 consists of the CO_2 cylinder, a pressure gauge (M1), a non-return valve (NRV), a metering valve (MV1), and a pressure relief valve (PRV) set at 15 MPa for this series of experiments. This rig part is connected by a metal hose to the main section (Section 2). The pressure vessel (PV), highlighted on the right of Fig. 1, consists of an upper stainless-steel cylinder and a lower short pipe; the external diameter is 4.8 cm for the former and 2.5 cm for the latter. After the vessel is separately cooled down in a freezer at 253 K, the sample is placed in it and vertically connected to the rig. The vessel is assembled in a heating copper coil (HEC), in which a heating liquid circulator (LC) pumps a mixture of water and glycol. After the liquid CO_2 is weighed, the upper and lower parts of the metal coil with the vessel are insulated. It is important to note that this coil does not affect the weight measurement since it does not touch the vessel.

In Fig. 2, the process is illustrated on the CO_2 phase diagram. Liquid CO_2 flows from the cylinder (1a) to the vessel due to the pressure difference caused by the temperature gradient. After filling (1b), the pressure vessel is heated following the vapor-liquid equilibrium, passing the critical point (2), up to the working conditions in the supercritical region (3).

The total amount of CO_2 inside the vessel can be controlled by a high-resolution hanging scale (HS, resolution ±1 g), since all the main part is connected to it (delimited by the dashed line in Fig. 1) and isolated from the first part by the flexible metal hose. The system weight, constituted by the weight of the vessel, valves, gauge, heating coil, and piping, is zeroed to measure accurately the weight of CO_2. The maximum quantity that can be filled depends on the vessel capacity, which for the proposed rig is 0.15 L. At this stage, the metering valves MV2 and MV3 are closed. MV1 is kept open until the desired amount of liquid is weighed. Afterwards, the heat provided by the copper coil increases the temperature in the vessel and, therefore, the fluid pressure, monitored by the pressure gauge M2. Using this method, the maximum pressure that can be reached in the temperature range of this work was observed to be about 20 MPa. The heating of Section 2 is remotely controlled to match the set temperature with the value measured by the thermocouple (Tc) located inside the vessel.

2.3 Thermodynamics

2.3.1 Equation of State

In this work, the equation of state (EOS) used to calculate the properties of the involved systems is the Soave-Redlich-Kwong (SRK) equation (Eq. (1)), widely accepted for supercritical fluid applications [26, 27].

$$P = \frac{RT}{V-b} - \frac{a(T)}{V(V+b)} \tag{1}$$

Temperature (T)[1)], pressure (P), and molar volume (V) are expressed in K, MPa, and L mol^{-1}, respectively. R is the gas constant expressed in L MPa K^{-1}mol^{-1}. Here, the interaction factor $a(T)$ depends on the temperature:

$$a(T) = a'(T_c)\alpha(T) \tag{2}$$

where

$$a'(T_c) = 0.42748\frac{R^2T_c^2}{P_c} \tag{3}$$

1) List of symbols at the end of the paper.

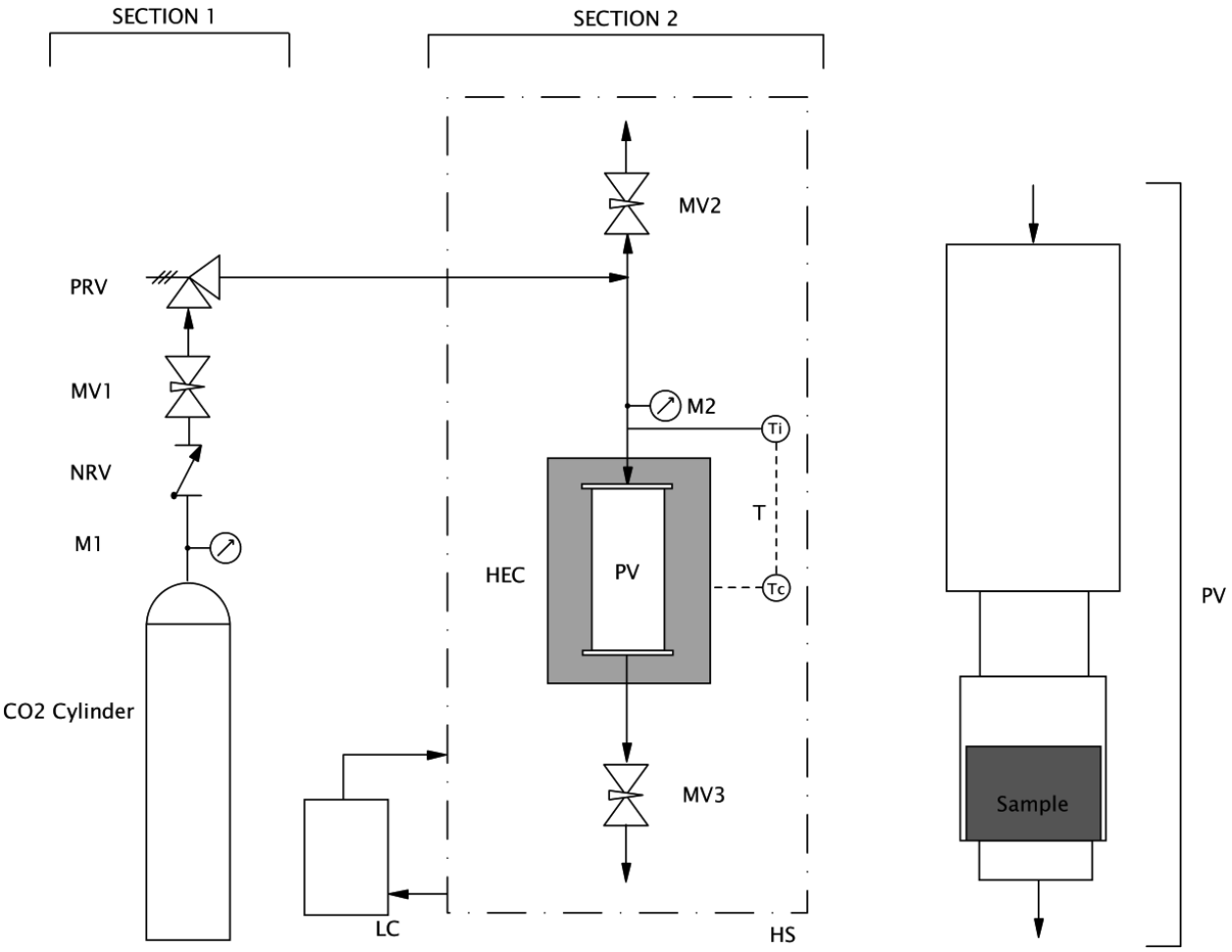

Figure 1. Schematic representation of the designed rig. The PV geometry is highlighted on the right. Solvents or active compounds are placed below the sample.

$$\alpha(T) = \left[1 + \left(0.480 + 1.574\omega - 0.176\omega^2\right)\left(1 - \sqrt{\frac{T}{T_c}}\right)\right]^2 \tag{4}$$

The co-volume b can be calculated as:

$$b = 0.08664\frac{RT_c}{P_c} \tag{5}$$

In these formulas, the subscript c means that it is related to the critical point, and ω is the acentric factor. For this EOS, the acentric factor ω is 0.239, T_c is 304.13 K, and P_c is equal to 7.38 MPa [27].

Brunner [27] discussed different EOSs, suggesting that both the ideal gas and the Van der Waals equations are not accurate for supercritical fluid applications. In effect, both equations oversimplify the system, leading to an incorrect estimation of the PVT (pressure, volume, temperature) behavior. Specifically, the ideal gas equation is well applicable only at high temperatures and low pressures, while the Van der Waals EOS is not adequate for practical applications for most substances [27].

The SRK EOS can still be used for the calculations even if the system is not a pure substance. In this case, the EOS is modified (Eq. (6)), combining the mixture parameters $a_m(T)$ and b, which can be defined by the quadratic mixing rules for a generic binary system (Eqs. (7) and (8)) [27]. The subscript m means modified.

$$P = \frac{RT}{V - b_m} - \frac{a_m(T)}{V(V + b_m)} \tag{6}$$

$$a_m(T) = X_1^2 a_{11}(T) + 2X_1X_2a_{12}(T) + X_2^2 a_{22}(T) \tag{7}$$

$$b_m = X_1^2 b_{11} + 2X_1X_2b_{12} + X_2^2 b_{22} \tag{8}$$

where X_i is the molar fraction in one phase, while both a_{ii} and b_{ii} are related to the pure components. The binary parameters $a_{12}(T)$ and b_{12} are expressed in Eqs. (9) and (10):

$$a_{12}(T) = \sqrt{a_{11}(T)a_{22}(T)}(1 - k_{12}) \tag{9}$$

$$b_{12} = 0.5(b_{11} + b_{22})(1 - l_{12}) \tag{10}$$

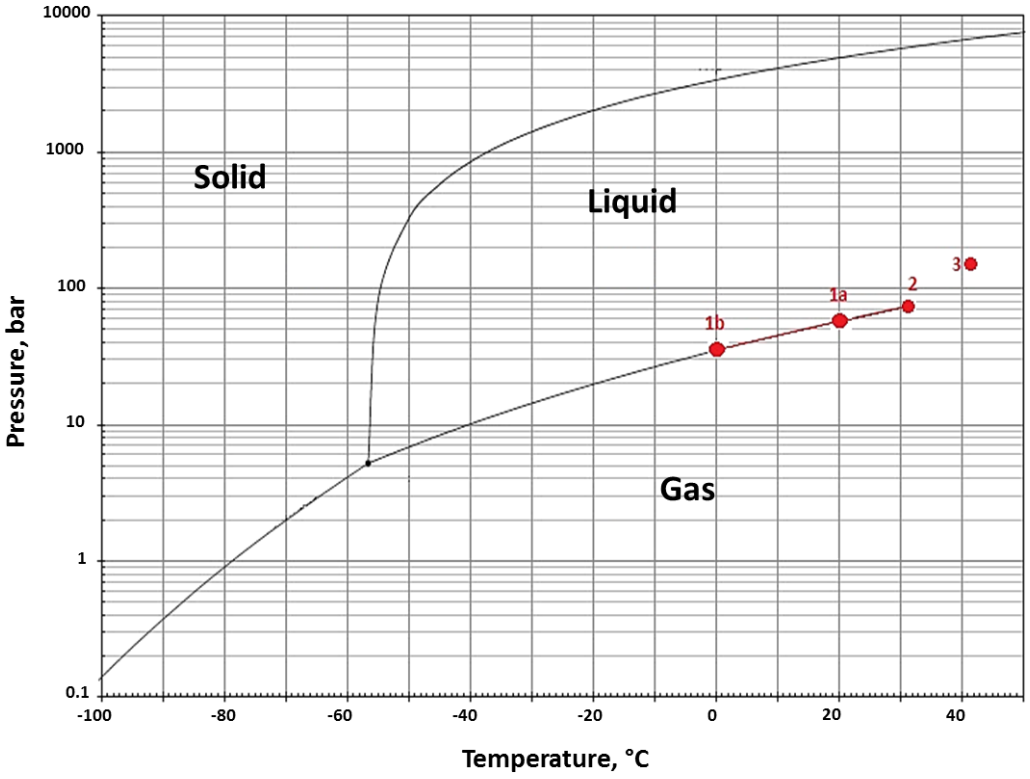

Figure 2. Process steps reported on the CO_2 phase diagram: (1a) CO_2 cylinder in vapor-liquid equilibrium, (1b) vessel filled with CO_2, (2) CO_2 critical point, (3) working conditions.

Both k_{12} and l_{12} are relatively smaller than 1. If both $a_{12}(T)$ and b_{12} are not known, they can be neglected [27]. Since ethanol is used in this work, the acentric factor ω and the critical temperature/pressure related to EtOH must be used to calculate both a_{ii} and b_{ii}. Specifically, the acentric factor is 0.644, T_c is 513.9 K, and P_c is 6.14 MPa. Both $a_{12}(T)$ and b_{12} have been set to zero to simplify the calculation method.

2.3.2 Method for Calculation of CO_2 Amount

Depending on the solute type and amount to solubilize, the quantity of CO_2 can require specific constraints to reach a homogeneous supercritical phase. Specifically, based on the solute volume, the process has to be designed calculating the minimum temperature and pressure. If the amount of solute is negligible, the simplest way is to directly use the suggested EOS. However, some solutes form a mixture with CO_2 with critical properties considerably different from those of the pure CO_2, especially higher critical pressure and temperature. In this case, the calculation needs specific thermodynamic restrictions.

For both cases, the initial step is the sample volume calculation to find the net free volume inside the vessel. The use of a pycnometer to measure the material density might simplify this estimation. If the system does not require specific constraints, the CO_2 mass can be worked out from Eq. (1). On the other hand, other substances soluble in CO_2 may interact with it forming a mixture with a different critical point. For example, ethanol is used in this study to displace water from the wet gels since it is poorly soluble in $scCO_2$ [28]. As a consequence, the critical point of the CO_2-EtOH system is higher than pure CO_2 [29, 30]. In this case, the critical temperature and pressure of the CO_2-EtOH system have to be lower than the working conditions to operate in completely developed supercritical conditions. In Fig. 3, the generic binary system CO_2-solvent [32] shows that to work in the supercritical state, the operating

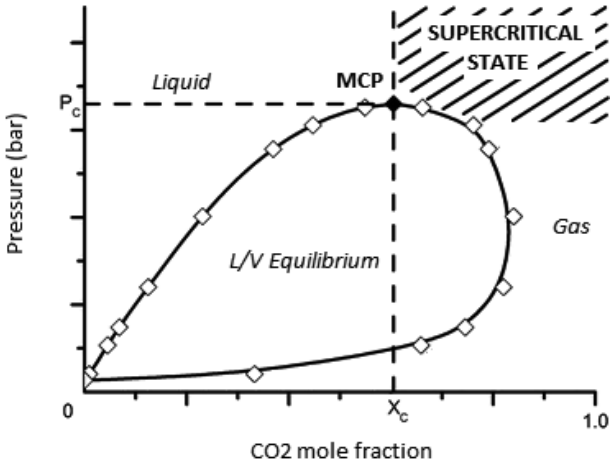

Figure 3. Generic isotherm phase diagram for a binary CO_2-solute system adapted from Akien and Poliakoff [31].

point should be located at a pressure value above the mixture critical point (MCP) of the binary system at a given temperature ($P > P_c$) and at a CO_2 molar fraction located on the right of the MCP ($X_1 > X_c$).

To calculate the amount of CO_2 needed to solubilize ethanol, an iterative procedure was used, as illustrated in Fig. 4. First, the working temperature (T_w) and pressure (P_w) were fixed. Since the moles of ethanol to remove (n_2) are known, it is necessary to hypothesize a value for CO_2 molar fraction (X_1). Therefore, the moles of CO_2 (n_1) can be obtained from Eq. (11):

$$n_1 = n_2 \frac{X_1}{(1 - X_1)} \tag{11}$$

Then, once calculated the total moles (n_1+n_2), it is possible to work out the molar volume V_m and the parameters a_m and b_m from Eqs. (7) and (8), respectively. Afterwards, from Eq. (6) it is possible to determine P. If this value corresponds to the working pressure ($P = P_w$), X_1 hypothesized is correct, otherwise a new value has to be fixed and the calculation process reiterated until convergence. For safety considerations, the maximum amount of liquid CO_2 should be lower than the total available volume in the vessel, to avoid an uncontrolled increase in pressure. The safety valve (PRV) prevents the rig from overpressure.

2.4 Experimental Procedures

2.4.1 Gel Drying

Gel samples were treated stepwise with alcoholic solutions at 25, 50, and 80 wt % and left in each concentration for 6 h. Finally, the samples were soaked in absolute ethanol for 24 h. The volume of the treated gel was measured in parallel by using the paraffin oil displacement method [33, 34] to precisely calculate both the net available volume in the vessel and the ethanol percentage. Afterwards, the amount of CO_2 can be obtained by the SRK EOS and applying the thermodynamic constraints previously discussed.

The effect of temperature was investigated at 313 and 323 K, while the working pressure was constantly at 10 MPa. After the system was heated, a drying time of 8 h was applied to promote the ethanol solubilization into the $scCO_2$. The venting stage was carried out opening MV3 at the bottom of the vessel and ensuring a low flow rate, i.e., less than 0.1 MPa min^{-1}, to maintain the temperature above the critical temperature and avoid the collapse of the material. Furthermore, the slow depressurization was carried out to limit the bubbling effect since the system becomes thermodynamically unstable [35]. At the end of the experiments, the produced aerogels were stored in a low-vacuum desiccator till characterization.

2.4.2 Freeze-Dried Gel Impregnation with Vitamin E

The freeze-dried gel consisting of HA/LA gellan gum 1:1 mixture at 2 wt % was placed in the vessel with 0.4 g of α-tocopherol on the bottom of the vessel. During this stage, the dried gel and the vitamin were not in direct contact. Two experiments were performed at 12 and 14 MPa, chosen as reference conditions [31]. The working temperature was fixed at 333 K for both experiments. After 24 h, chosen as reference time, the vessel was vented at a rate lower than 0.1 MPa min^{-1}. The sample was analyzed after complete depressurization.

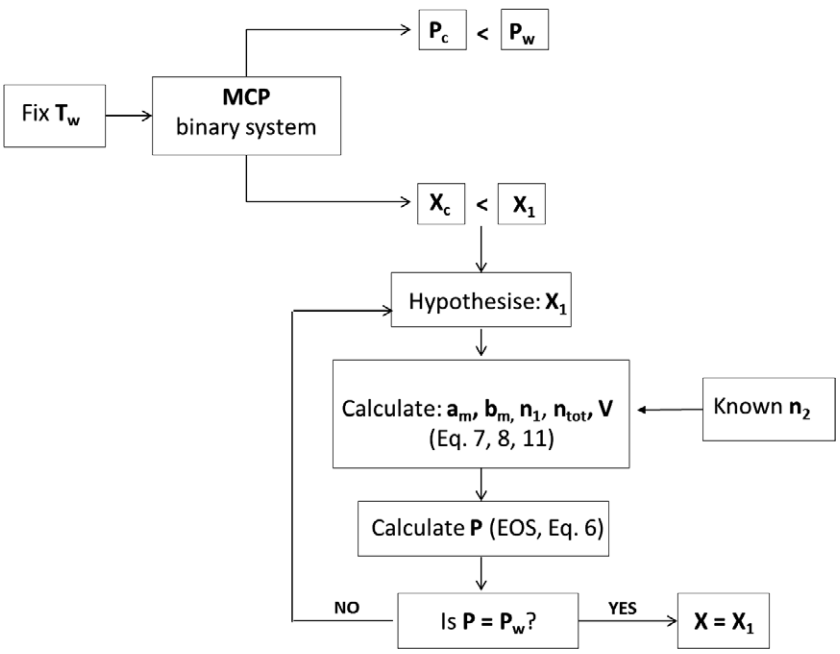

Figure 4. Proposed method for CO_2 calculation. The constraints are represented by "<". The subscript 1 is referred to CO_2, whereas 2 is referred to EtOH.

2.4.3 Caffeine Extraction

In the case of the coffee beans, they needed to be pretreated with water, as suggested in [36]. Firstly, a saturated caffeine solution was prepared by leaving the green Robusta coffee raw beans in water (1 g coffee for 2 g water) for 24 h in an ultrasonic bath to favor the mass transfer. The maximum amount of extracted caffeine was then calculated by UV-vis spectrophotometry, taking pure caffeine as a reference at a wavelength equal to 296 nm. Afterwards, the coffee beans to be processed were soaked for 1 h in this saturated solution to allow water to penetrate into the structure, yet limiting the caffeine loss by osmosis. The $scCO_2$ extraction was carried out at 313 K and 11 MPa, i.e., milder conditions [31] than those generally used in industrial processes [37], partially filling the bottom of the vessel with 4 mL of distilled water, separated from the sample by a metal grid. Same conditions were applied to black tea leaves, although no pretreatment was nec-

essary. Both the processes were performed for 8 h, followed by depressurization at the rate lower than 0.1 MPa min^{-1}.

2.5 Characterization Methods

2.5.1 Gel Drying

The aerogel microstructure was analyzed by X-ray micro-computed tomography (mCT) [38, 39]. High-resolution mCT was performed on a Skyscan 1172 (Bruker, Belgium). Without any chemical fixation or sample preparation, this system provides a complete 3D bulk reconstruction. The acquisition mode can be set at a maximum current of 96 µA and voltage of 100 kV. The CT-analyzer (1.7.0.0) was employed to obtain both a qualitative and quantitative analysis. After 2D cross-sectional binarization into black and white images, the overall porosity and the pore size distribution can be measured.

2.5.2 Freeze-Dried Gel Impregnation with Vitamin E

The amount of α-tocopherol absorbed in the substrate was calculated by weighing the sample before and after the process. As a further method of validation, UV-vis spectrophotometry (Orion AquaMate, Thermoscientific, UK) was applied, after calibration at 292 nm, placing the sample in an aqueous medium and measuring the concentration of the released vitamin [16]. The loading was calculated according to the following Eq. (12):

$$\text{Loading } \% = \frac{\text{mass } \alpha - \text{tocopherol adsorbed}}{\text{total mass}} \times 100 \qquad (12)$$

Fourier transform infrared (FTIR) spectra were obtained via the Spectrum Two IR Spectrometer (Perkin Elmer, UK) in reflection mode at a resolution of 4 cm^{-1}. The scan wavenumber range was 4000–500 cm^{-1}, and 16 scan signals were averaged to reduce the noise.

2.5.3 Caffeine Extraction

The concentration of caffeine in the obtained solution was analyzed by means of the UV-vis spectrophotometer, selecting the wavelength at 296 nm. The collected results were compared with data from literature [31].

2.6 Cost Analysis

A qualitative analysis was carried out to compare the setup and running costs of the proposed rig with a semicontinuous and a classic batch rig, using 0.15 L as a reference for the vessel capacity. The setup costs were estimated on the basis of current quotations, while the running costs were calculated considering the average energy requirements for each configuration and the amount of CO_2 employed during the processes.

3 Results and Discussion

3.1 Gel Drying

The CO_2 amount was calculated by the proposed method in Fig. 4. Before drying using $scCO_2$, the ethanol pretreatment was performed, leading to the sample dehydration before the actual process. The supercritical fluid technology was applied to remove the liquid from the sample to obtain a solid matrix, avoiding its collapse, which usually occurs with traditional drying because of the capillary-induced tensile stresses [40]. In effect, the photograph in Fig. 5 shows that downstream the drying process the cylindrical shape is preserved. Although some shrinkage occurred, the structure did not collapse.

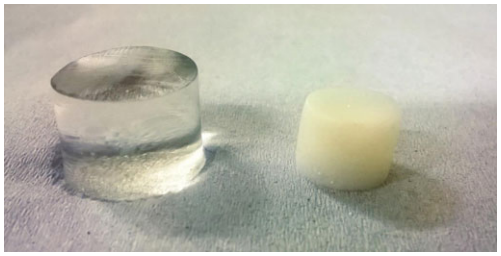

Figure 5. Photo of LA gellan gum gel (left) and aerogel (right).

Furthermore, from a microstructural point of view, it seems that no considerable differences rose within the working temperature range since both the shape and the shrinkage were comparable. The quantitative analysis provided a total porosity value equal to 28.8 ± 9.1 % at 323 K; at 313 K the porosity was within the same range. The considerable standard deviation was dependent on the large random pores generated during the drying process, as it was possible to notice from the pore size distribution (Fig. 6).

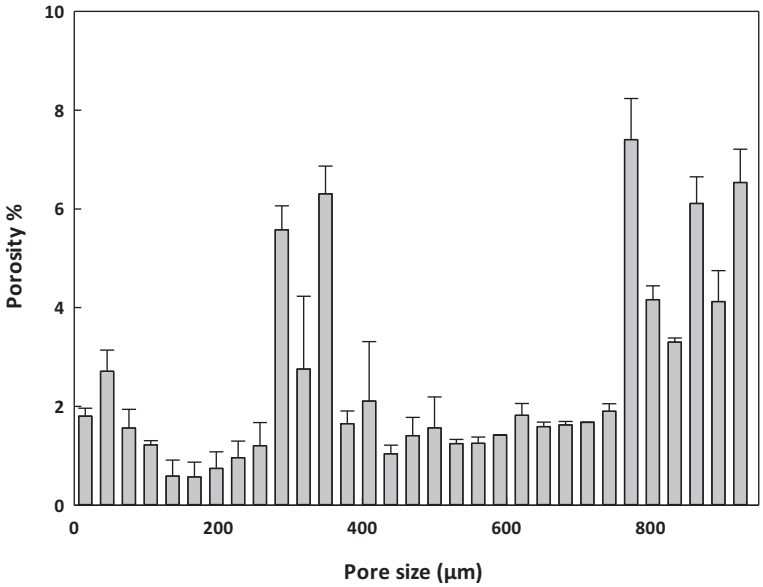

Figure 6. Pore distribution after $scCO_2$ drying (at 323 K and 10.0 MPa).

3.2 Freeze-Dried Gel Impregnation with Vitamin E

Solubility data allow determining the saturation conditions at fixed temperature and pressure. In particular, at 333 K and 12 MPa the molar solubility of α-tocopherol in $scCO_2$ is equal to 200×10^{-6}, whereas at 333 K and 14 MPa it is equal to 300×10^{-6} [41]. To assess the effectiveness of the designed rig also for supercritical impregnation, experiments of α-tocopherol adsorption in a porous gellan substrate were conducted at 333 K and the effect of the operating pressure was investigated. When the operating pressure was fixed at 12 MPa, α-tocopherol was impregnated, with a mean loading equal to 16.7 %. As expected from the solubility data, increasing the pressure at 14 MPa, the amount of absorbed vitamin increased, with a mean loading equal to 17.7 %.

FTIR analyses were performed to identify possible interactions between α-tocopherol and the hydrocolloid in the loaded gels. FTIR spectra of the unprocessed vitamin and gellan and processed α-tocopherol/gellan are reported in Fig. 7. The spectrum of unprocessed α-tocopherol shows adsorption bands at: 917 cm^{-1} OH bending, 1087 cm^{-1} in-plane bending of phenyl, 1158 cm^{-1} CH_2 wag, 1369 cm^{-1} CH_3 bending, 1465 cm^{-1} C–C stretching, and in the range 2800–3000 cm^{-1} stretching vibration of the C–H groups [16, 42]. The HA/LA gellan gum spectrum shows absorption bands at: 1017 cm^{-1} C=O stretching, 1413 cm^{-1} symmetric COO^- stretching, 1613 cm^{-1} asymmetric COO^- stretching, 2917 cm^{-1} C–H stretching, and in the range 3020–3660 cm^{-1} OH stretching [43]. The spectrum of the loaded gel confirms the occurred impregnation and indicates the presence of HA/LA gellan gum and α-tocopherol since the characteristic peaks of both compounds are present.

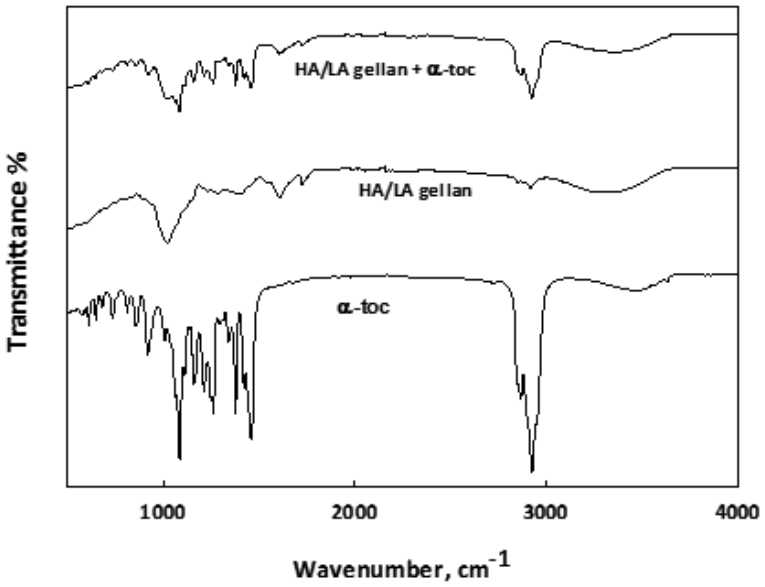

Figure 7. FTIR spectra of HA/LA gellan, α-tocopherol, and HA/LA gellan + α-tocopherol.

3.3 Caffeine Extraction

The extraction of caffeine from green coffee beans and black tea leaves was carried out in the presence of water [44]. In this case, it was not necessary to reach a homogeneous supercritical phase and, therefore, the SRK equation was used without applying any constraints. After the process at 313 K and 11 MPa, the collected solution was analyzed to calculate the amount of solubilized caffeine, as reported in Tab. 1. These values are in agreement with the literature data on caffeine solubilization in $scCO_2$ [45, 46], within the same order of magnitude. Interestingly, the amount of caffeine from green coffee beans is slightly lower than the quantity collected from black tea leaves. This was likely to be related to the different material morphology and structure. In effect, the rigid matrix of the coffee beans might represent a resistance for $scCO_2$ to penetrate and for the caffeine molecule to leave the material.

Table 1. Experimental caffeine concentration expressed as a molar fraction after extraction in supercritical CO_2.

Material	$y\times10^{-6}$ [–]
Green coffee beans	36.2
Black tea leaves	56.9

3.4 Cost Analysis

3.4.1 Setup Costs

As stated in the Introduction, SCF technologies are generally considered expensive due to the high investment costs. In the batch rig proposed in this work, these costs are considerably reduced. In literature, specific data related to the costs of these components are not available because they depend on the brand, the size, and the flow rate. However, on the basis of current quotations obtained from companies, it is possible to make a qualitative evaluation. A vessel with an internal volume equal to 150 mL was used as a reference for the calculations. If the total cost related to piping, valves, and manometers is defined with a cost index *C*, it is possible to estimate the cost index of the other components in comparison with it, as reported in Tab. 2.

From these approximate data it is possible to assess that the cost of the batch rig proposed in this work is about 3*C* (rows a, e, and g in Tab. 2), while the cost of a semicontinuous rig and a classic batch rig is about 10–14*C* (rows a and c–e). These estimations considered the use of a stainless-steel cylinder and a short pipe as a pressure vessel (see Sect. 2.2). The cost of a batch rig without pumps but equipped with quartz windows, which necessarily need to be fitted in a high-pressure vessel, is about 8–9*C* (rows a, b, e, and f). Therefore, the cost of the

Table 2. Cost indexes of the different components that can be part of a rig equipped with a 150-mL vessel.

	Equipment	Cost indexes
a	Piping, cylinder, valves, and manometers	*C*
b	High-pressure vessel	5–6*C*
c	High-pressure pump	6–8*C*
d	Pump cooling system	2–4*C*
e	Heating system	*C*
f	Quartz windows	*C*
g	Hanging scale + freezer	*C*

proposed rig is about 3–5 times lower than a semicontinuous and a classic batch rig, and about 3 times lower than a batch rig with quartz windows.

3.4.2 Running Costs

To have a general overview about the energy saving related to the proposed rig, a quantitative evaluation of the energetic costs was carried out in comparison with the classic batch rig and a semicontinuous rig, both equipped with a pump and a chiller. For this purpose, $scCO_2$ gel drying was considered as a reference process using a 150-mL vessel for the calculations. Usually, a semicontinuous process consists of the following steps: preliminary cooling to reach the chiller setpoint; pressurization of the vessel pumping $scCO_2$; stabilization of the operating conditions, i.e., pressure, temperature, and CO_2 flow rate; drying; depressurization (in the last no electric energy involved). In the classic batch process, the step related to the stabilization is missing since once the operating pressure is reached, the pump is switched off. In the proposed batch process, the pressurization step is performed without the use of pumps and the preliminary cooling of the vessel is carried out by using a dedicated freezer.

In Tab. 3, the average energy requirements of the main rig devices are reported. To estimate the energy consumption required by each configuration (proposed, classic batch, and semicontinuous rigs), the average times of each process step are presented in Tab. 4; these data were taken from the literature related to gel drying [47–49].

The energy consumptions of the three configurations are summarized in Tab. 5. The calculations were carried out considering the lowest energy requirement for each device from the ranges reported in Tab. 3. Similarly, for the semicontinuous rig, the lower pressurization and drying times were considered (Tab. 4). The comparison of the total energy consumption of the three configurations shows that the proposed rig allows a cost reduction of about 72 % with respect to the semicontinuous rig and about 33 % compared to the classic batch. Consequently, considering an average aerogel weight equal to 50 mg, it is possible to assess that the energy demand to produce the same amount of final product is 55 kJ mg^{-1} for the proposed rig, 82 kJ mg^{-1} for the classic batch rig, and 194 kJ mg^{-1} for the semicontinuous rig.

Another important factor to take into account is the amount of CO_2 employed during the process. Using the average process step times reported in Tab. 4, it is possible to calculate the total quantity of CO_2 required producing an aerogel. Specifically, for both batch rigs the required CO_2 mass is the same, while for the semicontinuous one it is considerably higher. As evidence, the drying working conditions of this study involve 50–80 g of CO_2 per process for both the proposed and classic batch rigs, whereas for the semicontinuous rig, supposing an average flow rate of 10–20 g min^{-1} [4, 16], the CO_2 quantity is about 2500–5000 g.

Table 3. Current energy requirements of the rig devices.

Equipment	Energy consumption [W]
High-pressure pump	180–750
Pump cooling system	200–1500
Freezer	25–40
Heating system	85–1100

Table 4. Average process step times needed for a rig equipped with a 150-mL vessel.

Process steps	Novel batch rig	Classic batch rig	Semicontinuous rig
Preliminary cooling [min]	120	120	120
Pressurization [min]	20	5–10	5–10
Stabilization [min]	0	0	15
Drying [min]	480	480	240–300

Table 5. Energy consumption calculation for each process step for a rig equipped with a 150-mL vessel.

	Novel batch rig	Classic batch rig	Semicontinuous rig
Cooling [kJ]	180	1500	5280
Heating [kJ]	2550	2474	1632
Pumping [kJ]	0	54	2808
Total energy consumption [kJ]	2730	4078	9720

4 Conclusions

A cost-reduced batch plant for supercritical fluid-assisted processes was proposed. It has been demonstrated that the designed plant is characterized by high flexibility since it is able

to adapt to different supercritical CO_2 applications, such as gel drying, impregnation, and extraction. It has been evaluated that the present rig allows a considerable reduction in both the set-up and running costs. On the basis of these results, it is possible to assess that the designed plant can be especially useful on laboratory scale to produce several products through different techniques but using the same rig and with reduced costs.

Acknowledgment

This research was funded by the Engineering and Physical Sciences Research Council (grant number EP/K030957/1) and the EPSRC Centre for Innovative Manufacturing in Food.

The authors have declared no conflict of interest.

Symbols used

a	[L^2mol^{-2}]	interaction factor
b	[$L\,mol^{-1}$]	co-volume
C	[–]	cost index
k	[–]	binary interaction parameter
l	[–]	binary interaction parameter
n	[mol]	number of moles
P	[MPa]	pressure
R	[$L\,MPa\,K^{-1}mol^{-1}$]	gas constant
T	[K]	temperature
V	[$L\,mol^{-1}$]	molar volume
X	[–]	molar fraction

Greek letters

α	[–]	constant
ω	[–]	acentric factor

Subscripts

c	critical
i	component i
m	modified
w	working

Abbreviations

α-toc	α-tocopherol
EOS	equation of state
EtOH	ethanol
FTIR	Fourier transform infrared
HA	high acyl
HEC	heating copper coil
HS	hanging scale
LA	low acyl
LC	liquid circulator
MCP	mixture critical point
mCT	micro-computed tomography
NRV	non-return valve
PRV	pressure relieve valve
PV	pressure vessel
$scCO_2$	supercritical carbon dioxide
SCF	supercritical fluid
SRK	Soave-Redlich-Kwong
Tc	thermocouple
VLE	vapor-liquid equilibria

References

[1] A. Tabernero, E. M. Martín del Valle, M. A. Galán, *Chem. Eng. Process.* **2012**, *60*, 9–25.
[2] V. Prosapio, I. De Marco, E. Reverchon, *Chem. Eng. J.* **2016**, *292*, 264–275.
[3] L. Liu, Z.-T. Liu, Z.-W. Liu, D. Xue, *Sci. China: Chem.* **2010**, *53*, 1586–1591.
[4] Z. K. Brown, P. J. Fryer, I. T. Norton, R. H. Bridson, *J. Supercrit. Fluids* **2010**, *54*, 89–95.
[5] Z. Ulker, C. Erkey, *J. Supercrit. Fluids* **2017**, *120*, 310–319.
[6] Y. Yokozaki, J. Sakabe, B. Ng, Y. Shimoyama, *Chem. Eng. Res. Des.* **2015**, *100*, 89–94.
[7] A. Baiano, M. A. Del Nobile, *Crit. Rev. Food Sci. Nutr.* **2016**, *56*, 2053–2068.
[8] S. Machmudah, K. Kitada, M. Sasaki, M. Goto, J. Munemasa, M. Yamagata, *Ind. Eng. Chem. Res.* **2011**, *50*, 2227–2235.
[9] R. H. Walters, B. Bhatnagar, S. Tchessalov, K.-I. Izutsu, K. Tsumoto, S. Ohtake, *J. Pharm. Sci.* **2014**, *103*, 2673–2695.
[10] R. Singh, M. K. Singh, S. Bhartiya, A. Singh, D. K. Kohli, P. C. Ghosh, S. Meenakshi, P. K. Gupta, *Int. J. Hydrogen Energy* **2017**, *42*, 11110–11117.
[11] S. He, X. Chen, *J. Non-Cryst. Solids* **2017**, *463*, 6–11.
[12] C. Domingo, in *Supercritical Fluid Nanotechnology* (Eds: C. Domingo, P. Subra-Paternault), Pan Stanford Publishing, Singapore **2015**, 1–18.
[13] M. Golubovic, S. H. Van Hateren, M. Ottens, G. J. Witkamp, L. A. M. Van Der Wielen, *Biotechnol. Bioeng.* **2007**, *98*, 1209–1218.
[14] D. Villanueva-Bermejo, G. Reglero, T. Fornari, *Trends Food Sci. Technol.* **2017**, *62*, 1–12.
[15] M. Pantić, P. Kotnik, Ž. Knez, Z. Novak, *J. Supercrit. Fluids* **2016**, *118*, 171–177.
[16] I. De Marco, E. Reverchon, *Chem. Eng. Res. Des.* **2017**, *119*, 221–230.
[17] M. Perrut, *J. Supercrit. Fluids* **2012**, *66*, 359–371.
[18] P. López-Domínguez, A. M. López-Periago, F. J. Fernández-Porras, J. Fraile, G. Tobias, C. Domingo, *J. CO2 Util.* **2017**, *18*, 147.
[19] V. Prosapio, E. Reverchon, I. De Marco, *Powder Technol.* **2016**, *292*, 140–148.
[20] V. Prosapio, E. Reverchon, I. De Marco, *J. Supercrit. Fluids* **2016**, *118*, 19–26.
[21] E. Zera, *Ph.D. Thesis*, University of Trento **2016**.
[22] M. Maiwald, G. M. Schneider, *J. Supercrit. Fluids* **1995**, *8*, 25–29.
[23] J. K. Lee, S. X. Yao, G. Li, M. B. Jun, P. C. Lee, *Polymer Rev.* **2017**, *57*, 695–747.
[24] R. Campardelli, E. Reverchon, I. De Marco, *J. Supercrit. Fluids* **2017**, *130*, 273–281.
[25] G. A. T. Sevilla, M. M. Hussain, *IEEE J. Emerging Sel. Top. Circuits Syst.* **2017**, *7*, 147–160.

[26] A. Sabirzyanov, A. Il'in, A. Akhunov, F. Gumerov, *High Temp.* **2000**, *40*, 203–206.
[27] G. Brunner, *Gas Extraction*, Springer, Heidelberg **1994**.
[28] G. Brunner, *J. Food Eng.* **2005**, *67*, 21–33.
[29] S.-D. Yeo, S.-J. Park, J.-W. Kim, J.-C. Kim, *J. Chem. Eng. Data* **2000**, *45*, 932–935.
[30] T. W. Furlong, *M.Sc. Thesis*, University of Massachusetts Amherst **2011**.
[31] R. B. Gupta, J.-J. Shim, *Solubility in Supercritical Carbon Dioxide*, CRC Press, Boca Raton, FL **2006**.
[32] G. R. Akien, M. Poliakoff, *Green Chem.* **2009**, *11*, 1083–1100.
[33] J. Del Valle, T. Cuadros, J. Aguilera, *Food Res. Int.* **1998**, *31*, 191–204.
[34] Z. Yan, M. J. Sousa-Gallagher, F. A. R. Oliveira, *J. Food Eng.* **2008**, *84*, 430–440.
[35] F. Mayinger, *Chem. Eng. Process.* **1988**, *23*, 1–11.
[36] H. Peker, M. Srinivasan, J. Smith, B. J. McCoy, *AIChE J.* **1992**, *38*, 761–770.
[37] I. De Marco, S. Riemma, R. Iannone, *J. Supercrit. Fluids* **2018**, *133*, 393–400.
[38] M. Cassanelli, I. Norton, T. Mills, *Food Hydrocolloids* **2018**, *75*, 51–61.
[39] T. Nissilä, S. S. Karhula, S. Saarakkala, K. Oksman, *Compos. Sci. Technol.* **2018**, *155*, 64–71.
[40] G. W. Scherer, *J. Am. Ceram. Soc.* **1990**, *73*, 3–14.
[41] C.-C. Chen, C.-M. J. Chang, P.-W. Yang, *Fluid Phase Equilib.* **2000**, *175*, 107–115.
[42] V. Prosapio, E. Reverchon, I. De Marco, *J. CO2 Util.* **2017**, *19*, 230–237.
[43] J. Silva-Correia, J. M. Oliveira, S. G. Caridade, J. T. Oliveira, R. A. Sousa, J. F. Mano, R. L. Reis, *J. Tissue Eng. Regener. Med.* **2011**, *5*, e97–e107.
[44] E. Stahl, K.-W. Quirin, D. Gerard, *Dense Gases for Extraction and Refining*, Springer, Heidelberg **2012**.
[45] G. I. Burgos-Solórzano, J. F. Brennecke, M. A. Stadtherr, *Fluid Phase Equilib.* **2004**, *220*, 55–67.
[46] S. Li, G. Varadarajan, S. Hartland, *Fluid Phase Equilib.* **1991**, *68*, 263–280.
[47] I. De Marco, S. Miranda, S. Riemma, R. Iannone, *Chem. Eng. Trans.* **2016**, *49*, 319–324.
[48] M. Dowson, M. Grogan, T. Birks, D. Harrison, S. Craig, *Appl. Energy* **2012**, *97*, 396–404.
[49] D. Ciftci, A. Ubeyitogullari, R. R. Huerta, O. N. Ciftci, R. A. Flores, M. D. A. Saldaña, *J. Supercrit. Fluids* **2017**, *127*, 137–145.

